The Journal of Neuroscience, July 1, 2001, *21*(13):4593–4599

The Presynaptic Function of Mouse Cochlear Inner Hair Cells during Development of Hearing

Dirk Beutner and Tobias Moser

Department of Membrane Biophysics, Max Planck Institute for Biophysical Chemistry, Am Fassberg, 37077 Göttingen, Germany, and Department of Otolaryngology, Göttingen University Medical School, Robert Koch Strasse, 37073 Göttingen, Germany

Before mice start to hear at approximately postnatal day 10, their cochlear inner hair cells (IHCs) spontaneously generate Ca^{2+} action potentials. Therefore, immature IHCs could stimulate the auditory pathway, provided that they were already competent for transmitter release. Here, we combined patch-clamp capacitance measurements and fluorimetric $[Ca^{2+}]_i$ recordings to study the presynaptic function of IHCs during cochlear maturation. Ca^{2+}-dependent exocytosis and subsequent endocytic membrane retrieval were already observed near the date of birth. Ca^{2+} action potentials triggered exocytosis in immature IHCs, which probably activates the auditory pathway before it becomes responsive to sound. IHCs underwent profound changes in Ca^{2+}-channel expression and secretion during their postnatal development. Ca^{2+}-channel expression increased toward the end of the first week, providing for large secretory responses during this period and thereafter declined to reach mature levels. The efficacy whereby Ca^{2+} influx triggers exocytosis increased toward maturation, such that vesicle fusion caused by a given Ca^{2+} current occurred faster in mature IHCs. The observed changes in Ca^{2+}-channel expression and synaptic efficacy probably reflected the ongoing synaptogenesis in IHCs that had been described previously in morphological studies.

Key words: synapse; exocytosis; hair cell; cochlea; capacitance; calcium

Mice are born deaf and start to hear during the second postnatal week (Mikaelian and Ruben, 1965; Ehret, 1985). During postnatal maturation, inner hair cells (IHCs), the primary sensory cells of the cochlea, undergo massive changes in their electrical and morphological properties. The immature pattern of ion channel expression permits electrical activity to take place in IHCs from newborn mice, whereas mature IHCs are restricted to graded membrane potential changes. The spontaneous action potentials (APs) are primarily mediated by Ca^{2+} channels and disappear around the onset of hearing because of the expression of a Ca^{2+}-activated potassium channel (Kros et al., 1998). The electrical activity of IHCs could stimulate the auditory nerve, provided that action potentials trigger exocytosis of transmitter in immature IHCs. Indeed, patterned spontaneous neuronal activity has been observed in the immature auditory pathway of some species (Walsh and McGee, 1988; Gummer and Mark, 1994; Lippe, 1994), as well as during hair cell regeneration after cochlear damage in chick (Salvi et al., 1994; Lippe, 1995). Patterned spontaneous activity is a hallmark of the developing nervous system and probably underlies the refinement and maintenance of neuronal connections (for review, see Katz and Shatz, 1996). The early activity in the auditory system is essential for the maintenance of the auditory pathway because deafferentiation causes massive neuronal cell death in the auditory brainstem (Tierney et al., 1997; Mostafapour et al., 2000). So far, there is little functional evidence that the activity of immature IHCs could stimulate the auditory pathway. Active zones are present in immature IHCs (Kikuchi and Hilding, 1965; Sobkowicz and Rose, 1983), and glutamate receptor channels (Luo et al., 1995; Knipper et al., 1997) are expressed in auditory nerve fibers of the developing organ of Corti. However, it remained unclear whether synaptic transmission at the afferent synapses is functional before the onset of hearing (Sobkowicz et al., 1982).

Here, we investigated the presynaptic function of mouse IHCs during cochlear maturation and tested the efficiency of action potentials as triggers for exocytosis. To study Ca^{2+} currents and exocytosis at the different developmental stages, we performed patch-clamp measurements of membrane current and capacitance (C_m) on IHCs from isolated semi-intact organs of Corti and combined them with fura-2 recordings of intracellular calcium ($[Ca^{2+}]_i$). We showed that mouse IHCs are ready for Ca^{2+}-dependent exocytosis at birth. Action potentials elicit exocytosis in immature IHCs. Before the onset of hearing, IHCs pass through a stage of strong exocytic activity attributable to increased expression of Ca^{2+} channels at a time when the highest number of synaptic ribbons is observed during synaptogenesis (Sobkowicz et al., 1986). Toward the onset of hearing, the amount of Ca^{2+} channel declines, and stimulus–secretion coupling improves.

MATERIALS AND METHODS

Whole-cell recordings. IHCs from the apical coil of freshly dissected organs of Corti from Naval Medical Research Institute (NMRI) mice of the specified age [hearing mice, postnatal day 14 (P14) to P25] were patch clamped at their basolateral face at room temperature (20–25°C). Pipette solutions for voltage-clamp experiments contained (in mM): 145 Cs-

Received Feb. 12, 2001; revised April 11, 2001; accepted April 13, 2001.

This work was supported by Deutsche Forschungsgemeinschaft and university grants to T.M. We thank Dr. E. Neher for his generous support and helpful discussions throughout this project. We would like to thank Andreas Brandt for fruitful discussions, Drs. E. Neher, T. Voets, R. Schneggenburger, and H. Sobkowicz for their comments on this manuscript, and Michael Pilot for excellent technical assistance.

Correspondence should be addressed to Tobias Moser, Department of Otolaryngology, Göttingen University Medical School, Robert Koch Strasse, 37073 Göttingen, Germany. E-mail: tmoser@gwdg.de.

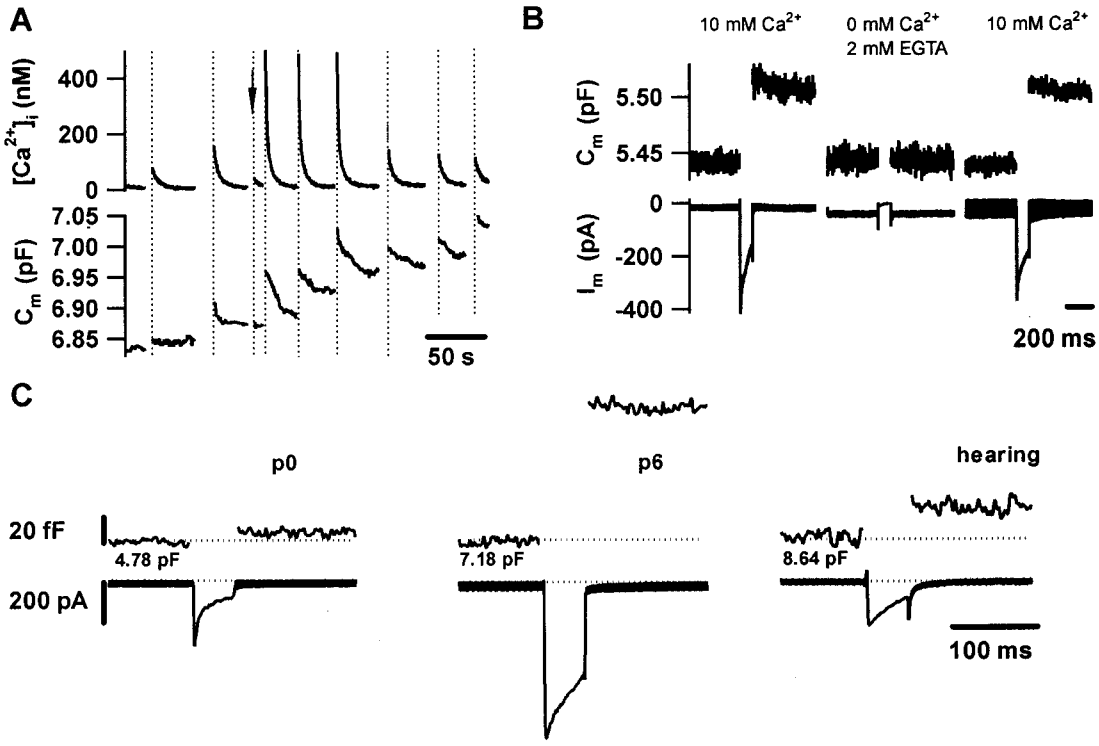

Figure 1. Ca^{2+}-dependent exocytosis can be evoked by depolarizations long before the onset of hearing. *A* shows $[Ca^{2+}]_i$ (*top panel*) and C_m (*bottom panel*) of an IHC from a P2 mouse at low time resolution. In response to long depolarizations (200 and 500 msec), sizable increases in C_m (exocytosis) and in $[Ca^{2+}]_i$ were observed. Shorter depolarizations resulted in much smaller responses (*arrow*, 50 msec). The subsequent decline in C_m most likely reflects endocytic membrane retrieval. *B*, C_m (*top panel*) and membrane current (*bottom panel*) of an IHC from a P6 mouse in response to 100 msec long depolarizations to −5 mV in the presence or absence of extracellular Ca^{2+} (Ca^{2+}-free Ringer containing 2 mM Ca^{2+}-free EGTA and 3 mM $MgCl_2$). C_m increments were inhibited by abolition of the Ca^{2+} influx and restored on readdition of Ca^{2+}. *C*, Representative Ca^{2+} currents (*bottom panel*) and C_m increments (*top panel*) of IHCs from different developmental stages to a 50 msec long depolarization to −5 mV. Baseline capacitance values are indicated below each *trace*.

gluconate, 8 NaCl, 10 CsOH-HEPES, 1 $MgCl_2$, 2 MgATP, 0.3 GTP. Free and Ca^{2+}-loaded EGTA was added in equal amounts of 5 mM, and NaCl was partially replaced by TEA (13 mM; Fluka, Buchs, Switzerland) for the whole-cell experiments of Figures 3*C* and 4. For perforated-patch experiments, amphotericin B (250 μg/ml) was added. For current-clamp recordings, Cs salts were replaced by the corresponding K^+ salts, and fura-2 (0.1 mM) was added to the pipette solution. The extracellular solution contained (in mM): 140 NaCl, 2.8 KCl, 1 $MgCl_2$, 10 NaOH-HEPES, 10 D-glucose, pH 7.2. For voltage-clamp experiments, NaCl was partially replaced by TEA (35 mM; Fluka). Extracellular $[Ca^{2+}]_o$ was 10 mM usually, but 2 mM for AP measurements. Solution changes were achieved by bath exchange. EPC-9 amplifiers (Heka Elektronik, Lambrecht/Pfalz, Germany) controlled by Pulse software (Heka) were used for measurements. All voltages were corrected for liquid junction potentials (−10 mV). For Figure 2, Ca^{2+} current amplitudes were measured 5 msec after the maximal inward current to avoid bias by any rapidly inactivating sodium currents. Ca^{2+} current integrals were calculated from the total depolarization-evoked inward current, including Ca^{2+} tail currents. Usually, no leak subtraction was performed. Instead, we excluded cells with a holding current exceeding −40 pA at −80 mV from analysis. Currents resembling the kinetics of tetrodotoxin-sensitive sodium currents were rarely observed in IHCs from neonatal NMRI mice and were absent after postnatal day 4. Therefore, tetrodotoxin was not regularly used in our experiments. $[Ca^{2+}]_i$ was measured by fura-2 fluorimetry (100 μM fura-2 potassium salt) using excitation at 360 and 390 nm and calculating $[Ca^{2+}]_i$ from the fluorescence ratio according to Grynkiewicz et al. (1985). Means are expressed ± SEM.

Capacitance measurements. We measured C_m using the Lindau-Neher technique (Lindau and Neher, 1988), implemented in the software-lockin module of Pulse combined with compensation of pipette and resting cell capacitances by the EPC-9 compensation circuitries. A 1 kHz, 70 mV peak-to-peak sinusoid was applied at a DC holding potential of approximately −80 mV. For the impedance analysis, the reversal potential of the DC was set to the reversal potential of the slow tail currents following the depolarizations as described previously (Moser and Beutner, 2000). The access resistances ranged from 5 to 14 MΩ (values after 200 sec of recording, random sample of 24 recordings) for standard whole-cell recordings and from 7 to 28 MΩ (values after 200 sec of recording, random sample of 13 cells) for perforated-patch recordings. Data analysis was performed using IGOR Pro-software (WaveMetrics Inc., Lake Oswego, OR). ΔC_m was estimated as the difference of the mean C_m over 400 msec after the end of the depolarization (the initial 30 msec were skipped) and the mean prepulse capacitance (400 msec).

RESULTS

Development of presynaptic Ca^{2+} current and secretory responses

Depolarization of immature IHCs caused Ca^{2+} entry, which triggered transient C_m increments and elevations of global $[Ca^{2+}]_i$. The C_m changes most likely reflect exocytic fusion of synaptic vesicles (C_m increase) with the plasma membrane and subsequent endocytic membrane retrieval (C_m decrease). Figure 1*A* shows a measurement of C_m and of global $[Ca^{2+}]_i$ in an IHC from a 2-d-old mouse (P2) that was stimulated by step depolarizations of variable duration to −5 mV. Robust C_m changes were elicited by long stimuli (200 and 500 msec), and smaller changes were elicited by short depolarizations (50 msec). The C_m increments evoked in IHCs before and after the onset of hearing were abolished on removal of extracellular Ca^{2+} (Fig. 1*B* and Moser and Beutner, 2000) as expected for Ca^{2+}-dependent fusion of synaptic vesicles with the plasma membrane. Voltage-gated Ca^{2+} current and exocytic capacitance changes (ΔC_m in fF) were observed as early as on the day of birth (Fig. 1*C*). However, the

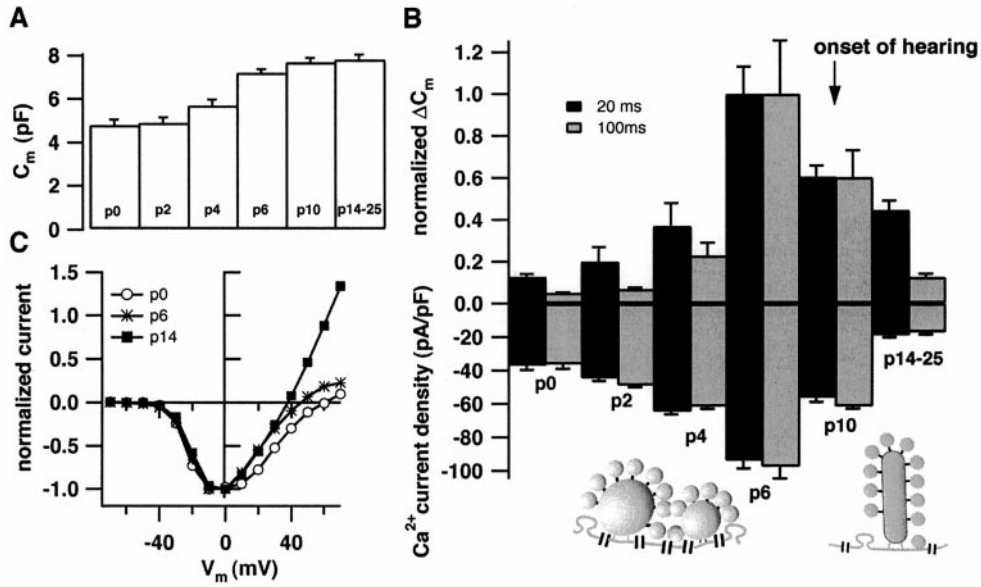

Figure 2. Developmental changes in Ca^{2+} current and exocytosis. *A* demonstrates the increase in basal cell capacitance during the course of maturation (P0, $n = 13$; P2, $n = 2$; P4, $n = 10$; P6, $n = 10$; P10, $n = 9$; and P14–P25, $n = 28$). *B* displays normalized ΔC_m-responses (*top panel*) to 20 or 100 msec long depolarizations to −5 mV (number of cells as in *A*, normalized to the average responses of P6 cells to either depolarization). The *bottom panel* shows the Ca^{2+} current densities for 20 and 100 msec depolarizations (peak Ca^{2+} currents normalized to the cell capacitance). The *arrow* indicates the onset of hearing. The *diagrams* depict the preferential abundance of multiple spherical bodies at the active zones of immature IHCs and the typical presence of only one plate-like ribbon at the mature afferent synapse. *C* displays representative current voltage relationships for three different developmental stages after subtracting the leak current (estimated by a linear fit to the hyperpolarized portion of the data).

exocytic responses at P0 were much smaller than those of IHCs from hearing mice. In addition to the Ca^{2+} current, we observed a voltage-dependent rapidly inactivating inward current in about half of the IHCs from early postnatal mice (P0–P4) (Fig. 1*C*). As expected for a neuronal voltage-activated Na^+ current, it was blocked by tetrodotoxin (data not shown). At the end of the first postnatal week, IHCs displayed very large Ca^{2+} currents and C_m increments (Fig. 1*C*). Analysis of capacitative currents did not reveal significant additional slow current components, arguing against electrical coupling among hair cells (data not shown).

Figure 2*A* shows that the resting cell capacitance increased during the postnatal development. This C_m rise probably reflected an increase in cell size. Amplitudes of Ca^{2+} current (*bottom bars*) and exocytic ΔC_m (*top bars*) recorded in the perforated-patch configuration from IHCs at the different developmental stages are displayed in Figure 2*B*. The *arrow* indicates the onset of hearing (Mikaelian and Ruben, 1965; Ehret, 1985). The schematic drawing of active zones emphasizes the fact that one active zone in immature IHCs commonly contains several round synaptic bodies, whereas mature synapses usually display only one plate-like ribbon (Sobkowicz et al., 1982). The ΔC_m responses to 20 and 100 msec depolarizations (*black* and *gray bars*, respectively) were normalized to the peak amplitudes that were observed at P6. Ca^{2+} currents were normalized to the cell capacitance (i.e., Ca^{2+} current density). There was a massive increase in both Ca^{2+} current density and amplitude of exocytic responses toward the end of the first postnatal week and a subsequent decline to lower levels in IHCs from hearing mice. Similar calcium currents were obtained in whole-cell experiments in which TEA (13 mM) was added to the pipette solution to secure the block of potentially contaminating outward currents. The amplitudes of the secretory responses to short depolarizations were much less reduced during development than those evoked by long stimuli. A detailed description of secretion kinetics at the different stages is provided below.

The normalized current–voltage relationships of IHCs recorded in the perforated-patch configuration at the different stages revealed a similar voltage dependence of Ca^{2+}-channel activation (Fig. 2*C*).

Developmental changes in secretion kinetics

The kinetics of exocytosis was analyzed by measuring C_m increments in response to depolarizations of different durations. Using this paradigm in IHCs from hearing mice, we previously described a small, fast secretory component and a robust slow phase of secretion with nearly constant rate for at least 1 sec of depolarization. The fast secretory component was resistant to high doses of the slow Ca^{2+} chelator EGTA, whereas the buffer largely suppressed the slow secretory component. The fast component most likely represents exocytosis of a small readily releasable pool (RRP) of vesicles that are docked closely to Ca^{2+} channels at the active zones and can be depleted within 30 msec of stimulation. Rapid replenishment of the depleted RRP, as well as exocytosis in parallel to the RRP release, could underlie the slow component (Moser and Beutner, 2000). These more slowly released vesicles could be docked to the plasma membrane at some distance from the Ca^{2+} channels, explaining their sensitivity to EGTA.

Figure 3, *A* and *B*, shows the results from perforated-patch experiments on cells from the different developmental stages. Neonatal (P0) IHCs secreted less than mature cells throughout the whole range of stimulus durations. The fast secretory component was still small in P4 IHCs (Fig. 3*B*), whereas a sizable slow secretory component was already observed at this stage (Fig. 3*A*). At the end of the first week, IHCs displayed high secretory rates during the slow component, so that it was hard to separate the two kinetic components in the data of P6 IHCs recorded in the perforated-patch configuration (Fig. 3*B*). A decline in secretory rate became evident when P6 IHCs were stimulated for >200 msec (Fig. 3*A*). A similar secretory behavior, albeit with lower maximal rate of the slow secretory component, was observed in P10 IHCs.

High doses of EGTA strongly suppressed the slow secretory component in IHCs of hearing mice, thus isolating the release of the RRP, which is resistant to at least 5 mM EGTA (Moser and Beutner, 2000). At the same concentration, EGTA also reduced the responses of immature IHCs to longer depolarizations, but to a lesser extent than in P14–P25 IHCs (Fig. 3*C, P6*). Nevertheless, we now could isolate the fast secretory component in P6 IHCs by

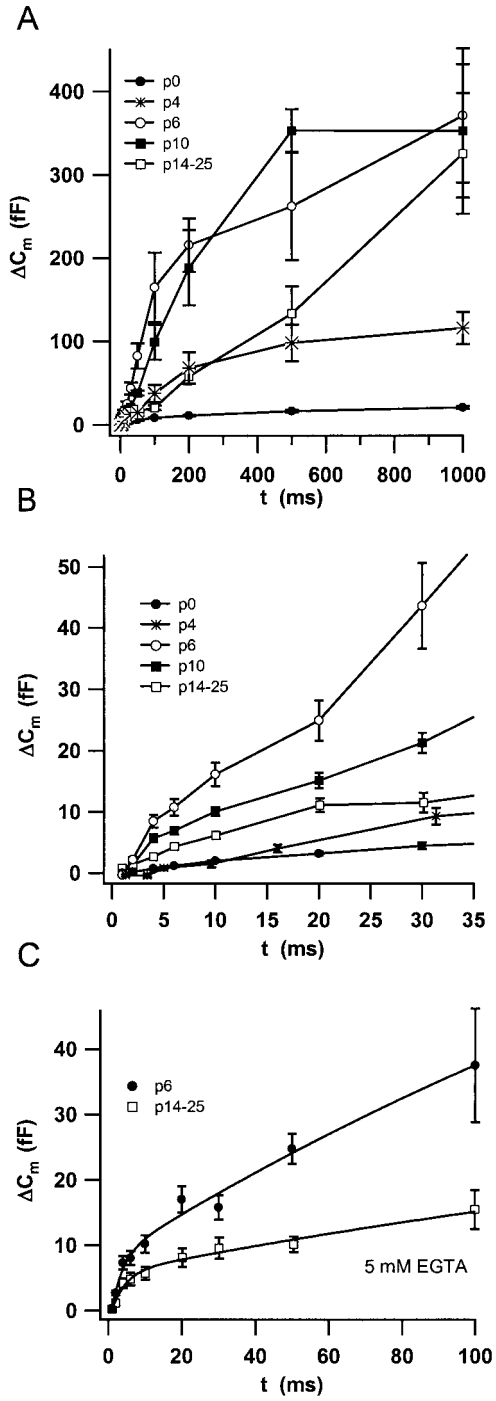

Figure 3. Changes in secretion kinetics during maturation. Secretion kinetics was investigated by measuring ΔC_m to depolarizations (to −5 mV) of different duration applied in random order. *A* plots the mean C_m responses recorded in the perforated-patch configuration in IHCs from the different stages ($n = 13$ cells for P0; $n = 10$ for P6; $n = 9$ for P10; and $n = 28$ for IHCs from hearing mice). *B* displays the first 30 msec of stimulation with higher resolution. *C* compares the ΔC_m of whole-cell experiments on IHCs from P6 and hearing mice in which we added a mixture of 5 mM Ca^{2+}-free EGTA and 5 mM Ca^{2+}-loaded EGTA to the pipette ($n = 9$ cells for P6; $n = 27$ for IHCs from P14–P25). The *solid lines* represent double exponential fits to the data to estimate size and release time constant of the readily releasable pool (see text).

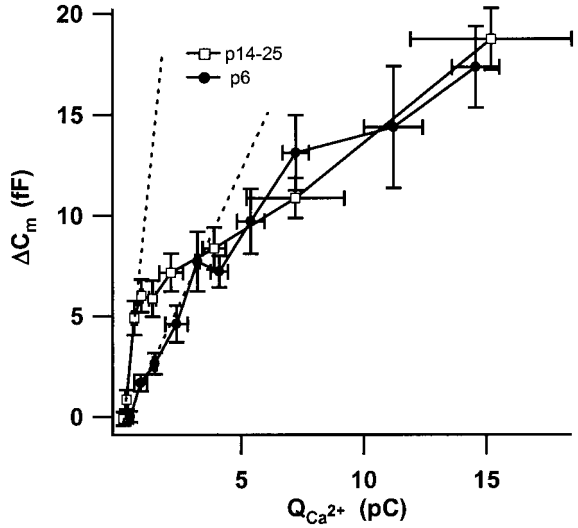

Figure 4. Ca^{2+} dependence of exocytosis during and after maturation. The plot relates secretory responses of 5 mM EGTA-buffered IHCs from P6 and P14–P25 mice to their Ca^{2+} current integrals (restricted to small integrals; $n = 9$ cells for P6 and $n = 27$ for P14–P25 IHCs). The *dashed lines* represent linear fits to the first three points of each data set.

double-exponential fitting to the data (first 100 msec of stimulation) (Fig. 3*C*, *solid lines*). The fast component (i.e., RRP release) had a size of 10.8 fF and a time constant of 3 msec for the P6 IHCs. Assuming a single vesicle capacitance of 37 aF (Lenzi et al., 1999), this corresponds to fusion of 290 readily releasable vesicles. Using the same approach, we estimated an RRP of 7.4 fF (~200 vesicles) fusing with a time constant of 3.9 msec (Fig. 3*C*) for IHCs from P14–P25 mice.

Changes in the coupling of Ca^{2+} influx to exocytosis

The RRP of P6 IHCs was released only slightly faster than that of IHCs from hearing mice (3 vs 3.9 msec) (Fig. 3*C*), despite the much stronger Ca^{2+} influx into the immature cells. This indicates a less efficient stimulus secretion coupling for the release of fusion competent vesicles in immature IHCs. To further test this idea, we investigated the efficiency of Ca^{2+} current for eliciting exocytosis in IHCs from P6 and P14–P25 mice. Figure 4 plots the exocytic responses versus their corresponding Ca^{2+} current integrals for strongly EGTA-buffered IHCs. The maximal slope, approximated by a linear fit to the first three data points was much larger in cells from hearing mice (11.5 vs 2.6 fF/pC). The amount of exocytosis per given calcium influx was significantly different ($p < 0.001$) when comparing responses with up to 2.5 pC but statistically indistinguishable above 5 pC. The overlap of the data for larger amounts of Ca^{2+} influx suggests that a common Ca^{2+}-dependent mechanism underlies the slow component during and after completion of maturation. Similar overlap was observed for the analogous plots from perforated-patch experiments on P6, P10, and P14–P25 IHCs for integrals >5 pC, whereas the slow component of P0 to P4 IHCs displayed shallower dependencies on the Ca^{2+} influx (data not shown).

Ca^{2+} action potentials trigger exocytosis in immature IHCs

Figure 5*A* shows a representative tight-seal whole-cell recording of the membrane potential from a P6 IHC displaying high-amplitude, broad action potentials in the absence of any holding current injection. The APs strictly depended on extracellular

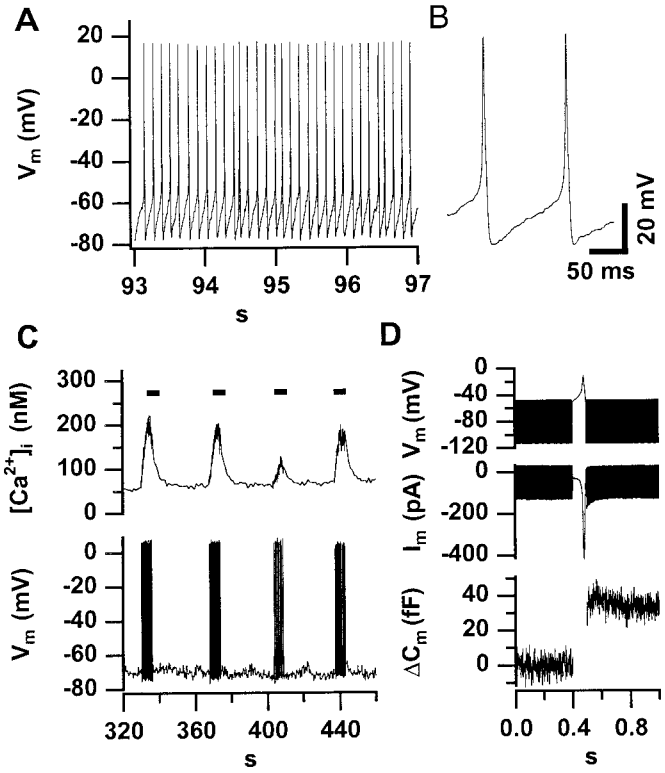

Figure 5. Spontaneous action potentials trigger exocytosis and increase $[Ca^{2+}]_i$ in immature IHCs. *A* displays an AP train recorded in the whole-cell configuration in the absence of any holding current from a representative P6 IHC. In this particular cell, spontaneous activity was observed during the first 260 sec of the whole-cell recording. *B* displays two spontaneous APs from the same cell at higher time resolution. *C* shows a low-time resolution plot of $[Ca^{2+}]_i$ and membrane potential (V_m) of an IHC in which we applied 10 pA of depolarizing current for short intervals (indicated by *bars*) after spontaneous activity had ceased. *D* shows an average of three secretory responses of two IHCs from a P6 mouse to a single action potential. We used the voltage-clamp mode to measure capacitance before and after an AP-like voltage-waveform to −10 mV. The time periods of C_m measurements can be recognized from the band-like (sinusoidal) signals in the voltage and current *traces*.

Ca^{2+} (changing from the standard $[Ca^{2+}]_e$ of 2 mM to a Ca^{2+}-free bath solution abolished the APs; data not shown). They occurred with frequencies of up to 8 Hz (mean of 48 APs recorded from 4 cells during the first 200 sec: 6.1 ± 0.9 Hz). Figure 5*B* displays two spontaneous action potentials of the same cell at higher time resolution. On average, APs had a mean halfwidth of 7.2 ± 2.6 msec and an amplitude of 82.8 ± 10.2 mV starting from a potential of −62.5 ± 4.4 mV. Usually, spontaneous activity was present during the first minutes of a whole-cell recording and ceased later, probably because of run-down of Ca^{2+} current in the whole-cell configuration.

Figure 5*C* shows that trains of action potential elicited robust increases in $[Ca^{2+}]_i$. To test whether action potentials are sufficient to trigger exocytosis, we stimulated IHCs with voltage waveforms mimicking recorded action potentials. Figure 5*D* illustrates the robust C_m response (average data from two P6 IHCs) even to a single AP-like voltage waveform. From the kinetics of exocytosis in IHCs at the different developmental stages (Fig. 3*A*,*B*), we conclude that trains of the broad Ca^{2+} action potentials are sufficient to trigger exocytosis before activity ceases around the onset of hearing.

DISCUSSION

In this study, we show that Ca^{2+}-dependent exocytosis and endocytosis are already functional in mouse IHCs near the date of birth. Therefore, acquisition of presynaptic Ca^{2+}-dependent exocytosis by immature IHCs does not seem to determine the onset of hearing. However, the observed strengthening of stimulus secretion coupling may be required for establishing the faithful information transfer at the mature afferent synapse. The developmental changes in Ca^{2+} current amplitude and exocytic behavior most likely reflect changes in number and arrangement of presynaptic active zones of IHCs. We postulate that the transmitter release driven by the spontaneous activity of immature IHCs is important for the maintenance and development of IHCs, their afferent synapses, and the ascending auditory pathway.

Relating the physiological data to morphological findings during synaptogenesis in IHCs

The differences in Ca^{2+} current density observed during development probably reflect changes in expression levels of L-type Ca^{2+} channels, because the L-type current dominates the Ca^{2+} current of IHCs throughout the postnatal period (Platzer et al., 2000). The finding of a similar voltage dependence of Ca^{2+} current activation before and after the onset of hearing (Fig. 2*C*) further supports the assumption of developmental changes in abundance of one Ca^{2+}-channel type. The increase in Ca^{2+}-channel density and exocytic responses toward the end of the first postnatal week parallels the formation of multiribbon active zones that are characteristic for the ongoing synaptogenesis during this time period (Sobkowicz et al., 1982). Indeed, the number of ribbons reaches its peak at the end of the first week and declines during further development (Sobkowicz et al., 1986) when the permanent innervation has been established (Echteler, 1992). Therefore, the decline in the Ca^{2+}-channel density after the end of the first postnatal week probably reflects the loss of active zones and/or the transition from multiple to one ribbon-active zones. However, we cannot exclude that, in addition, a more diffuse expression of a large number of Ca^{2+} channels in immature IHCs is being replaced by a selective targeting of fewer Ca^{2+} channels to the active zones.

Excessive generation of active zones not only is seen in the developing cochlea but also occurs during reactive synaptogenesis after cochlear damage. For example, multiribbon synapse formation has been observed after excitotoxic cochlear injury (Puel et al., 1995) as well as after cutting the auditory nerve (Sobkowicz et al., 1998). Therefore, the assembly of multiple active zones facing one postsynaptic terminal may generally be required for proper synapse formation. The fivefold decrease in Ca^{2+} current density (from P6 to P14–P25) contrasts with the only 1.5-fold reduction in the number of readily releasable vesicles residing close to Ca^{2+} channels (P6, 290 vesicles; P14–P25, 200 vesicles). This could indicate a different arrangement of Ca^{2+} channels and release sites in the immature cells and/or fewer release sites at the active zones in the immature cells. Different release properties at the different stages would not be too surprising because Sobkowicz et al. (1982) show that the developing synapses change in many aspects in addition to the varying number of ribbons per active zone. The finding of similar RRP fusion time constants in IHCs from P6 and hearing mice (Fig. 3*C*), despite the much larger Ca^{2+} influx at P6, indicates a higher efficiency of Ca^{2+} influx for triggering secretion in mature IHCs. This is most obvious from the steeper dependence of the RRP release on Ca^{2+} influx in

P14–P25 IHCs (Fig. 4). Such efficient stimulus secretion coupling is probably essential for the rapid changes in release rate required for the faithful transfer of timing information at the mature afferent synapse. The developmental improvement could result from changes in the positional arrangement of Ca^{2+} channels and release sites. Alternatively, it could reflect an increased intrinsic release probability caused by changes in the molecular composition of the fusion apparatus during maturation.

When longer depolarizations were applied, we observed a major overlap of the exocytic responses from P6 and hearing animals when plotted versus the corresponding Ca^{2+} current integral (Fig. 4). This indicates a similar Ca^{2+} dependence of the slow secretory component among IHCs from the different developmental stages. IHCs from the postnatal days 6 and 10 showed a decline in secretory rate (depression) (Fig. 3*A*) within 1 sec of stimulation, which was not evident in the data obtained from P14–P25 IHCs. This depression probably reflects exhaustion of a large pool of slowly releasable vesicles. The maximal secretory rate of the "slow" secretory component was much larger in P6 and P10 IHCs than in P14–P25 IHCs. This was, most likely, caused by an earlier recruitment of the slowly releasable vesicles by the larger Ca^{2+} influx in the immature IHCs. The different kinetics of the slow secretory component is therefore the major reason for the varying amplitudes of exocytic responses to long depolarizations among P6, P10, and P14–P25 IHCs (Fig. 2*B*). Such dependence of the secretory rate during the slow secretory phase on the Ca^{2+} influx may reflect a need for intracellular Ca^{2+} diffusion to the release sites (Voets et al., 1999) or a slow priming process, which can be accelerated by Ca^{2+} (Smith et al., 1998; Gomis et al., 1999). A similar Ca^{2+} dependence of the slow secretory component has also been observed in bipolar nerve terminals in which Ca^{2+} influx was manipulated experimentally (Sakaba et al., 1997).

Physiological implications of the early activity of IHCs

Our presynaptic measurements suggest that the electrically active immature IHCs trigger or modulate the activity of the immature auditory nerve. However, our data cannot prove whether IHCs also fire action potentials *in vivo* and whether the auditory nerve fibers respond properly to the presynaptic exocytosis of transmitter before the onset of hearing. A finding supporting our hypothesis is that the spiking pattern in the immature auditory pathway changes from bursting to continuous when the efferent control of IHCs is abolished (Walsh and McGee, 1988). Recently, this has been suggested to result from relief of cholinergic inhibition of IHC electrical activity (Glowatzki and Fuchs, 2000). Interestingly, the bursting rate in the immature auditory pathway varies among projections of different tonotopical locations (Lippe, 1995). It is possible that efferent fibers set the length of spiking periods for a number of tonotopically neighboring hair cells. The physiological significance of the presensory auditory nerve activity is demonstrated by the finding that deafferentiation causes massive neuronal cell death in the auditory brainstem (Tierney et al., 1997; Mostafapour et al., 2000). In addition to stimulating auditory nerve activity, IHC activity may release neurotrophic factors. This could be essential for the maintenance of spiral ganglion neurons (Erkman et al., 1996; Knipper et al., 1997).

The presensory IHC activity seems also to be important for the differentiation and maintenance of the IHCs themselves. Bursts of IHC APs cause repetitive elevations of the global cytosolic $[Ca^{2+}]_i$ (Fig. 5*B*), and their repetition frequency may be under efferent control *in vivo* (see above). Such Ca^{2+} oscillations could regulate a multitude of cellular functions, such as gene expression (Gu and Spitzer, 1995; Dolmetsch et al., 1998; Li et al., 1998). Knock-out of L-type Ca^{2+} channels, which is very likely to abolish the electrical activity of IHCs, leads to degeneration of hair cells as well as afferent nerve fibers (Platzer et al., 2000).

REFERENCES

Dolmetsch RE, Xu K, Lewis RS (1998) Calcium oscillations increase the efficiency and specificity of gene expression. Nature 392:933–936.

Echteler SM (1992) Developmental segregation in the afferent projections to mammalian auditory hair cells. Proc Natl Acad Sci USA 89:6324–6327.

Ehret G (1985) Behavioural studies on auditory development in mammals in relation to higher nervous system functioning. Acta Otolaryngol [Suppl] 421:31–40.

Erkman L, McEvilly RJ, Luo L, Ryan AK, Hooshmand F, O'Connell SM, Keithley EM, Rapaport DH, Ryan AF, Rosenfeld MG (1996) Role of transcription factors Brn-3.1 and Brn-3.2 in auditory and visual system development. Nature 381:603–606.

Glowatzki E, Fuchs PA (2000) Cholinergic synaptic inhibition of inner hair cells in the neonatal mammalian cochlea. Science 288:2366–2368.

Gomis A, Burrone J, Lagnado L (1999) Two actions of calcium regulate the supply of releasable vesicles at the ribbon synapse of retinal bipolar cells. J Neurosci 19:6309–6317.

Grynkiewicz G, Poenie M, Tsien RY (1985) A new generation of Ca2+ indicators with greatly improved fluorescence properties. J Biol Chem 260:3440–3450.

Gu X, Spitzer NC (1995) Distinct aspects of neuronal differentiation encoded by frequency of spontaneous Ca2+ transients. Nature 375:784–787.

Gummer AW, Mark RF (1994) Patterned neural activity in brain stem auditory areas of a prehearing mammal, the tammar wallaby (*Macropus eugenii*). NeuroReport 5:685–688.

Katz LC, Shatz CJ (1996) Synaptic activity and the construction of cortical circuits. Science 274:1133–1138.

Kikuchi K, Hilding D (1965) The development of the organ of Corti in the mouse. Acta Otolaryngol 60:207–222.

Knipper M, Kopschall I, Rohbock K, Kopke AKE, Bonk I, Zimmermann U, Zenner H (1997) Transient expression of NMDA receptors during rearrangement of AMPA-receptor-expressing fibers in the developing inner ear. Cell Tissue Res 287:23–41.

Kros CJ, Ruppersberg JP, Rusch A (1998) Expression of a potassium current in inner hair cells during development of hearing in mice. Nature 394:281–284.

Lenzi D, Runyeon JW, Crum J, Ellisman MH, Roberts WM (1999) Synaptic vesicle populations in saccular hair cells reconstructed by electron tomography. J Neurosci 19:119–132.

Li W, Llopis J, Whitney M, Zlokarnik G, Tsien RY (1998) Cell-permeant caged InsP3 ester shows that Ca2+ spike frequency can optimize gene expression. Nature 392:936–941.

Lindau M, Neher E (1988) Patch-clamp techniques for time-resolved capacitance measurements in single cells. Pflügers Arch 411:137–146.

Lippe WR (1994) Rhythmic spontaneous activity in the developing avian auditory system. J Neurosci 14:1486–1495.

Lippe WR (1995) Relationship between frequency of spontaneous bursting and tonotopic position in the developing avian auditory system. Brain Res 703:205–213.

Luo L, Brumm D, Ryan AF (1995) Distribution of non-NMDA glutamate receptor mRNAs in the developing rat cochlea. J Comp Neurol 361:372–382.

Mikaelian D, Ruben RJ (1965) Development of hearing in the normal CBA-J mouse. Acta Otolaryngol 59:451–461.

Moser T, Beutner D (2000) Kinetics of exocytosis and endocytosis at the cochlear inner hair cell afferent synapse of the mouse. Proc Natl Acad Sci USA 97:883–888.

Mostafapour SP, Cochran SL, Del Puerto NM, Rubel EW (2000) Patterns of cell death in mouse anteroventral cochlear nucleus neurons after unilateral cochlea removal. J Comp Neurol 426:561–571.

Platzer J, Engel J, Schrott-Fischer A, Stephan K, Bova S, Chen H, Zheng H, Striessnig J (2000) Congenital deafness and sinoatrial node dysfunction in mice lacking class D L-type Ca2+ channels. Cell 102:89–97.

Puel JL, Saffiedine S, Gervais d'Aldin C, Eybalin M, and Pujol R (1995) Synaptic regeneration and functional recovery after excitotoxic injury in the guinea pig cochlea. C R Acad Sci III 318:67–75.

Sakaba T, Tachibana M, Matsui K, Minami N (1997) Two components of transmitter release in retinal bipolar cells: exocytosis and mobilization of synaptic vesicles. Neurosci Res 27:357–370.

Salvi RJ, Saunders SS, Hashino E, Chen L (1994) Discharge patterns of chicken cochlear ganglion neurons following kanamycin-induced hair cell loss and regeneration. J Comp Physiol [A] 174:351–369.

Smith C, Moser T, Xu T, Neher E (1998) Cytosolic Ca2+ acts by two separate pathways to modulate the supply of release-competent vesicles in chromaffin cells. Neuron 20:1243–1253.

Sobkowicz HM, Rose JE (1983) Innervation of the organ of Corti of the fetal mouse in culture. In: Development of auditory and vestibular systems (Romand R, ed), pp 27–45. New York: Academic.

Sobkowicz HM, Rose JE, Scott GE, Slapnick SM (1982) Ribbon synapses in the developing intact and cultured organ of Corti in the mouse. J Neurosci 2:942–957.

Sobkowicz HM, Rose JE, Scott GL, Levenick CV (1986) Distribution of synaptic ribbons in the developing organ of Corti. J Neurocytol 15:693–714.

Sobkowicz HM, August BK, Slapnick SM, Luthy DF (1998) Terminal dendritic sprouting and reactive synaptogenesis in the postnatal organ of Corti in culture. J Comp Neurol 397:213–230.

Tierney TS, Russell FA, Moore DR (1997) Susceptibility of developing cochlear nucleus neurons to deafferentation-induced death abruptly ends just before the onset of hearing. J Comp Neurol 378:295–306.

Voets T, Neher E, Moser T (1999) Mechanisms underlying phasic and sustained secretion in chromaffin cells from mouse adrenal slices. Neuron 23:607–615.

Walsh EJ, McGee J (1988) Rhythmic discharge properties of caudal cochlear nucleus neurons during postnatal development in cats. Hear Res 36:233–247.